THE JOURNAL OF BIOLOGICAL CHEMISTRY VOL. 289, NO. 16, pp. 11497–11511, April 18, 2014

Phosphatidic Acid (PA)-preferring Phospholipase A_1 Regulates Mitochondrial Dynamics*

Received for publication, November 1, 2013, and in revised form, March 4, 2014 Published, JBC Papers in Press, March 5, 2014, DOI 10.1074/jbc.M113.531921

Takashi Baba[‡], Yuriko Kashiwagi[‡], Nagisa Arimitsu[‡], Takeshi Kogure[‡], Ayumi Edo[‡], Tomohiro Maruyama[‡], Kazuki Nakao[§], Hiroki Nakanishi[¶], Makoto Kinoshita[‖], Michael A. Frohman[**], Akitsugu Yamamoto[‡‡], and Katsuko Tani[‡1]

From the [‡]School of Life Sciences, Tokyo University of Pharmacy and Life Sciences, Hachioji, Tokyo 192-0392, Japan, the [§]RIKEN Center for Developmental Biology, 2-2-3 Minatojima-Minamimachi, Chuo-ku, Kobe 650-0047, Japan, the [¶]Research Center for Biosignal, Akita University, Akita 010-8543, Japan, the [‖]Division of Biological Science, Graduate School of Science, Nagoya University, Furo-cho, Chikusa-ku, Nagoya 464-8602, Japan, the [**]Department of Pharmacology and Center for Developmental Genetics, Stony Brook University, Stony Brook, New York 11794-5140, and the [‡‡]Faculty of Bioscience, Nagahama Institute of Bio-Science and Technology, Nagahama, Shiga 526-0829, Japan

Background: Phosphatidic acid (PA) is involved in membrane dynamics.
Results: PA-preferring phospholipase A_1 (PA-PLA_1) affects mitochondrial morphology in an activity-dependent manner. Gene disruption of PA-PLA_1 in mice causes sperm malformation due to mitochondrial organization defects.
Conclusion: PA-PLA_1 regulates mitochondrial dynamics.
Significance: We demonstrate an *in vivo* function of PA-PLA_1 and suggest a possible mechanism of PA regulation of the mitochondrial membrane.

Recent studies have suggested that phosphatidic acid (PA), a cone-shaped phospholipid that can generate negative curvature of lipid membranes, participates in mitochondrial fusion. However, precise mechanisms underling the production and consumption of PA on the mitochondrial surface are not fully understood. Phosphatidic acid-preferring phospholipase A_1 (PA-PLA_1)/DDHD1 is the first identified intracellular phospholipase A_1 and preferentially hydrolyzes PA *in vitro*. Its cellular and physiological functions have not been elucidated. In this study, we show that PA-PLA_1 regulates mitochondrial dynamics. PA-PLA_1, when ectopically expressed in HeLa cells, induced mitochondrial fragmentation, whereas its depletion caused mitochondrial elongation. The effects of PA-PLA_1 on mitochondrial morphology appear to counteract those of MitoPLD, a mitochondrion-localized phospholipase D that produces PA from cardiolipin. Consistent with high levels of expression of PA-PLA_1 in testis, PA-PLA_1 knock-out mice have a defect in sperm formation. In PA-PLA_1-deficient sperm, the mitochondrial structure is disorganized, and an abnormal gap structure exists between the middle and principal pieces. A flagellum is bent at that position, leading to a loss of motility. Our results suggest a possible mechanism of PA regulation of the mitochondrial membrane and demonstrate an *in vivo* function of PA-PLA_1 in the organization of mitochondria during spermiogenesis.

Phosphatidic acid (PA)[2] is a central intermediate for the synthesis of glycerophospholipids and triacylglycerol. Recent studies have indicated that PA is involved in a variety of physiological processes such as membrane trafficking and cell signaling. PA can be generated via several routes including the hydrolysis of phospholipids by phospholipase D (PLD), the phosphorylation of diacylglycerol by diacylglycerol kinase, and the acylation of lysophosphatidic acid (LPA) by lysophosphatidic acid acyltransferase (1, 2). PA can be metabolized to LPA by phospholipases A (PLA_1 and PLA_2) (3) and to diacylglycerol by PA phosphatases such as Lipin 1 (4). Moreover, PA acyl chains may undergo a cycle of deacylation and acylation by means of PLA_1/A_2 and lysophosphatidic acid acyltransferases, respectively, in the Lands cycle (3, 5).

Mitochondria are dynamic organelles, and their morphology is regulated by the balance between fusion and fission. These processes are mediated by GTPases: fusion of the outer and inner membranes is mediated by Mitofusin (Mfn) and Opa1, respectively, and fission is mediated by Drp1 (6). In mitochondria, PA can be generated from cardiolipin by the action of mitochondrial PLD (MitoPLD), a PLD family member found on the mitochondrial surface (7). Recent studies demonstrated that MitoPLD and Lipin 1 phosphatase reciprocally regulate the dynamics of mitochondria. It has been proposed that production of PA by MitoPLD facilitates Mfn-mediated fusion, whereas the consumption of PA and the production of diacylglycerol by Lipin 1 promote mitochondrial fission (8–10).

Intracellular PLA_1 ($iPLA_1$) proteins constitute a relatively recently discovered lipid-metabolizing enzyme family (11). Mammals have three $iPLA_1$ family members (phosphatidic acid-preferring phospholipase A_1 (PA-PLA_1)/DDHD1 (12),

* This work was supported in part by Grant-in-aid for Scientific Research 23570239 (to K. T.) from the Ministry of Education, Culture, Sports, Science and Technology of Japan.

[1] To whom correspondence should be addressed: School of Life Sciences, Tokyo University of Pharmacy and Life Sciences, 1432-1 Horinouchi, Hachioji, Tokyo, Japan 192-0392. Tel.: 81-42-676-6905; Fax: 81-42-676-5468; E-mail: tani@toyaku.ac.jp.

[2] The abbreviations used are: PA, phosphatidic acid; CCCP, carbonyl cyanide *m*-chlorophenylhydrazone; $iPLA_1$, intracellular phospholipase A_1; LPA, lysophosphatidic acid; mGPx4, mitochondrial glutathione peroxidase 4; MEF, mouse embryonic fibroblast; Mfn, Mitofusin; MitoPLD, mitochondrial PLD; PA-PLA_1, phosphatidic acid-preferring phospholipase A_1; PLD, phospholipase D; CMXRos, chloromethyl-X-rosamine; PABD, PA binding domain; EGFP, enhanced GFP.

KIAA0725p/DDHD2 (13), and p125/Sec23IP (14)). PA-PLA$_1$, which is the iPLA$_1$ first identified by Glomset and co-worker (15), preferentially hydrolyzes PA. PA-PLA$_1$ is highly expressed in brain and testis, especially in mature but not in newborn testis, raising the possibility that PA-PLA$_1$ is involved in spermatogenesis or sperm function (12, 15). But so far, the physiological role of PA-PLA$_1$ has not been elucidated. Recent human genetic approaches revealed that mutations in the *PA-PLA$_1$* gene cause hereditary spastic paraplegia (16), an inherited neurodegenerative disorder characterized by slowly progressive lower limb spasticity and weakness (17). Tesson *et al.* (16) indicated a possible link between lipid metabolism in mitochondria and the appearance of hereditary spastic paraplegia symptoms.

In this study, we showed that PA-PLA$_1$ regulates mitochondrial dynamics. Ablation of the *PA-PLA$_1$* gene caused defects in the organization of mitochondria during spermiogenesis, leading to sperm malformation and male subfertility.

EXPERIMENTAL PROCEDURES

Plasmid Construction—The mammalian expression plasmid for FLAG-tagged human PA-PLA$_1$ was described previously (18). Ser-537 in human PA-PLA$_1$ corresponds to the active site residue, Ser-540, in bovine PA-PLA$_1$ (12). The human PA-PLA$_1$ S537A mutant in which Ser-537 was replaced by Ala was constructed by site-directed mutagenesis. To express FLAG-tagged human PA-PLA$_1$ and PA-PLA$_1$ S537A in PA-PLA$_1$ siRNA-transfected cells, the siRNA targeting sequences were changed by PCR-based site-direct mutagenesis as follows: AAGAGTTGCCTGATGAACGAT to AGGAACTTCCGGACGAGCGCT (letters underlined indicate nucleotides changed) for the PA-PLA$_1$ siRNA5 site. The expression plasmids for the wild-type or mutant (H156N) MitoPLD, Raf1-PA binding domain (PABD)-EGFP, and Raf1-PABD mutant-EGFP were described previously (9). cDNAs encoding myc-tagged wild-type and mutant (H156N) MitoPLD were amplified by PCR and inserted into the pcDNA3 vector.

RNA Interference—The siRNA targeting sequences used for HeLa cells were as follows: Lamin A/C siRNA, CTGGACTTCCAGAAGAACA; PA-PLA$_1$ siRNA2, AAGCCACATTAGAAGACAAGC; PA-PLA$_1$ siRNA5, AAGAGTTGCCTGATGAACGAT; KIAA0725p siRNA2, GAAAGAAGATATTAAACTA; KIAA0725p siRNA3, GGAGAAAGTAGATAAGGAA. HeLa cells were transfected at a final concentration of 200 nM using Oligofectamine (Invitrogen) according to the manufacturer's protocol. Unless otherwise indicated, cells were fixed and processed at 72 h after transfection. The siRNA targeting sequences used for mouse embryonic fibroblasts (MEFs) were as follows: KIAA0725p siRNA1, GAAAGAAGATACTGAACCA; KIAA0725p siRNA5, GCGGATTGACTACGTGCTA. PA-PLA$_1$ siRNA used for MEFs were obtained from Invitrogen (PA-PLA$_1$1, MSS201695; PA-PLA$_1$2, MSS201696). MEFs were transfected at a final concentration of 100 nM using Lipofectamine RNAiMAX (Invitrogen) according to the manufacturer's protocol. AllStars Negative Control siRNA (Qiagen) was used as a control. Cells were fixed and processed at 72 h after transfection.

HeLa Cell Culture and Transfection—HeLa cells were maintained in α-modified Eagle's minimal essential medium supplemented with 10% fetal bovine serum, 2 mM L-glutamine, and penicillin/streptomycin. Plasmids were transfected using Lipofectamine 2000 reagent (Invitrogen) according to the manufacturer's protocol.

Analysis of the Mitochondrial Length—Cells were stained with an antibody against Tom20, and images were obtained by confocal microscopy and analyzed using ImageJ software. The average length of Tom20-positive tubules in the peripheral regions ($20 \times 20\ \mu m^2$) was estimated.

Antibodies and Probes—GST-tagged full-length human PA-PLA$_1$ was expressed in Sf9 cells and purified using glutathione beads. The purified protein was injected into BALB/c mice, and hybridoma cells producing antibodies against PA-PLA$_1$ were obtained according to the standard protocol. Culture supernatants were used for the immunostaining of testis sections. Polyclonal antibodies against α-tubulin and FLAG were purchased from Abcam and Sigma-Aldrich, respectively. A polyclonal antibody against SEPT4 was described previously (19). Monoclonal antibodies against cytochrome *c* and Tom20 were obtained from BD Transduction Laboratories. Monoclonal antibodies against Drp1, Mfn1, and Mfn2 were obtained from BD Transduction Laboratories, Abnova, and Abcam, respectively. FITC-conjugated goat anti-mouse and Texas Red-conjugated goat anti-rabbit antibodies were purchased from Jackson ImmunoResearch Laboratories. Alexa Fluor 350-conjugated goat anti-rabbit and anti-mouse antibodies, Alexa Fluor 488-conjugated goat anti-mouse antibody, MitoTracker Red CMXRos, and MitoTracker Deep Red FM were purchased from Invitrogen. Hoechst 33342 and protonophore carbonyl cyanide *m*-chlorophenylhydrazone (CCCP) were obtained from Thermo Scientific and Wako Chemicals, respectively.

Lipid Analysis by Mass Spectrometry—Cells were collected by gently scraping with a rubber policeman. Subcellular fractionation was performed essentially as described previously (20), and the mitochondrial fractions were used for the lipid analysis. Protein concentration was determined by the bicinchoninic acid method. Total lipids were extracted by the method of Bligh and Dyer (29). PA and LPA were separated from total lipids using a DEAE-cellulose column. LC-electrospray ionization-MS/MS analysis was performed using a TSQ-Vantage (Thermo Fisher Scientific, Waltham, MA) with an UltiMate 3000 LC system (Thermo Fisher Scientific) equipped with an HTC PAL autosampler (CTC Analytics, Zwingen, Switzerland). This MS system was controlled by Xcalibur software. PA and LPA were measured by selected reaction monitoring in the negative ion mode. The amounts of PA and LPA were determined from the ratio of the peak area of each PA and LPA species to that of internal standards (14:0/14:0 PA and 17:0 LPA).

Generation of PA-PLA$_1$ Knock-out Mice—A targeting vector (Clone PGS00049_B_D06) was obtained from the Knock-out Mouse Project (KOMP) Repository at the University of California Davis. The vector was electroporated into embryonic stem cells (TT2 cells). Two targeted cell lines were injected into ICR eight-cell stage embryos, and chimeric mice were obtained by the conventional method. All animal procedures and experiments were approved by the Animal Care Committee of Tokyo University of Pharmacy and Life Sciences and conducted according to the guidelines of the committee.

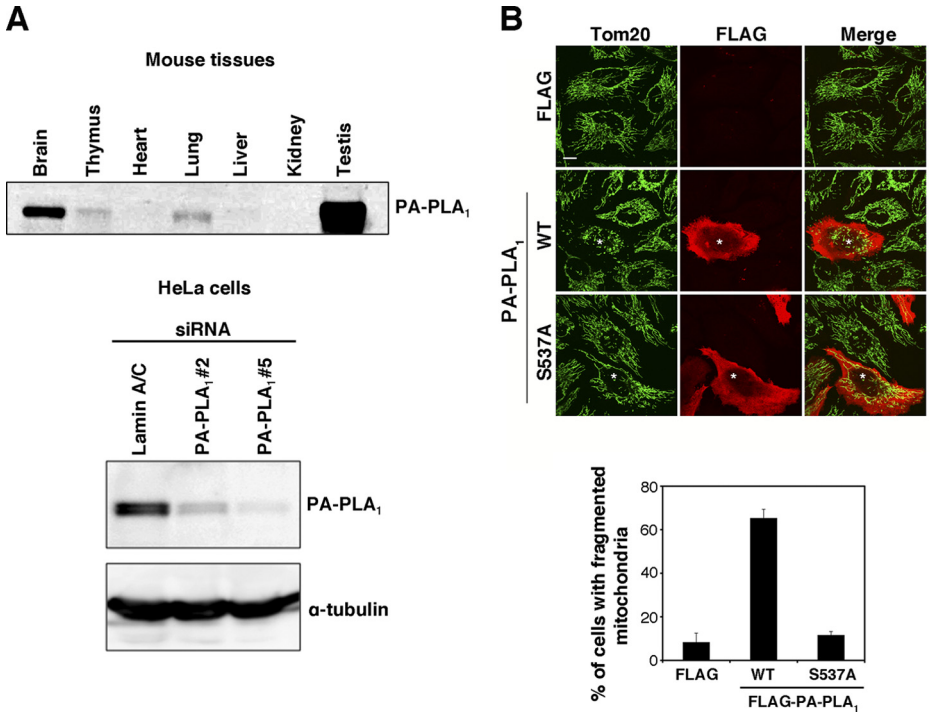

FIGURE 1. **PA-PLA$_1$ regulates mitochondrial dynamics.** *A*, lysates (50 μg each) of different mouse tissues (*upper panel*) and HeLa cells treated with Lamin A/C siRNA, PA-PLA$_1$ siRNA2, or PA-PLA$_1$ siRNA5 (*lower panel*) were analyzed by Western blotting with the indicated antibodies. *B*, HeLa cells were transfected with the empty FLAG plasmid (*top*), the plasmid encoding FLAG-PA-PLA$_1$ (*middle*), or the FLAG-PA-PLA$_1$ S537A mutant (*bottom*). At 24 h after transfection, cells were double stained with antibodies against FLAG and Tom20. Cells expressing FLAG-PA-PLA$_1$ or FLAG-PA-PLA$_1$ S537A mutant are indicated with *asterisks*. *Scale bar*, 10 μm. Quantitative data are shown at the *bottom*. Cells with fragmented mitochondria were counted under a fluorescence microscope. At least 100 cells were analyzed for each sample. Data represent the means ± S.D. for three independent experiments. *Error bars* represent S.D.

Histology—Mouse testes were fixed with 3.7% formaldehyde in PBS, dehydrated, and then embedded in paraffin. Paraffin sections (6 μm) were stained with hematoxylin and eosin (H&E) according to the standard protocol. For immunohistochemistry, testes were fixed with 4% paraformaldehyde in PBS and frozen in O.C.T compound (Tissue-Tek, Sakura, Japan). Cryosections (10 μm) were prepared and stained as described previously (21).

Preparation of Sperm—Cauda epididymis, caput epididymis, and testis were dissected in human tubal fluid medium and incubated with 5% CO_2 at 37 °C for 1 h. Released sperm were washed with PBS and spread on poly-L-lysine-coated coverslips. Then the sperm were fixed with 4% paraformaldehyde for 20 min and used for light microscopy and immunofluorescence analysis. For the motility assay, released sperm were observed under an Olympus IX70 microscope, and images were recorded using an Olympus DP70 charge-coupled device camera.

Immunofluorescence and Microscopic Analyses—Immunofluorescence images were analyzed as described previously (22, 23). An Olympus FluoView 1000 laser scanning microscope was used for confocal microscopy. For electron microscopic analysis, cauda epididymis was sequentially fixed with 2.5% glutaraldehyde in 0.1 M phosphate buffer (pH 7.4) and with 1% OsO_4 in the buffer. Electron microscopic analysis was performed as described previously (21).

Preparation of MEFs and Cell Culture—MEFs were isolated from E13.5 embryos by trypsinization and cultured in Dulbecco's modified Eagle's medium supplemented with 50 IU/ml penicillin, 50 μg/ml streptomycin, and 10% fetal calf serum. Two days after isolation, the cells were immortalized with SV40 large T antigen using a retrovirus expression system (24). The immortalized cells were cultured in medium containing 2 μg/ml puromycin.

RESULTS

PA-PLA$_1$ Is Involved in Mitochondrial Dynamics—PA-PLA$_1$ is predominantly expressed in mature testis and brain but also at low levels in other tissues including HeLa cells (Ref. 12 and Fig. 1*A*). To explore the function of PA-PLA$_1$ in mitochondrial dynamics, PA-PLA$_1$ with a FLAG tag was overexpressed in HeLa cells, and then mitochondrial morphology was examined by immunofluorescence microscopy. In control cells, mitochondria exhibited long tubular structures (Fig. 1*B*, *top row*). Upon overexpression of PA-PLA$_1$, the tubular structures became fragmented (*middle row*). Of note is that this morphological change is activity-dependent. Overexpression of the S537A mutant of human PA-PLA$_1$, which is equivalent to the S540A mutant of bovine PA-PLA$_1$ that lacks phospholipase A$_1$ activity (12), had no effect on mitochondrial morphology (*bottom row*).

Next, HeLa cells were treated with siRNA targeting PA-PLA$_1$, and then the morphology of mitochondria was examined. Western blotting verified the depletion of PA-PLA$_1$ (Fig. 1*A*, *lower panel*). In cells transfected with PA-PLA$_1$ siRNA2, elongation of the mitochondrial tubules was observed (Fig. 2*A*, *middle row*). In some cells, interconnected mitochondrial aggregates were detected in the perinuclear region (Fig. 2*A*, *middle row*, *right column*). A similar elongation and aggregation phenotype was observed for cells transfected with PA-

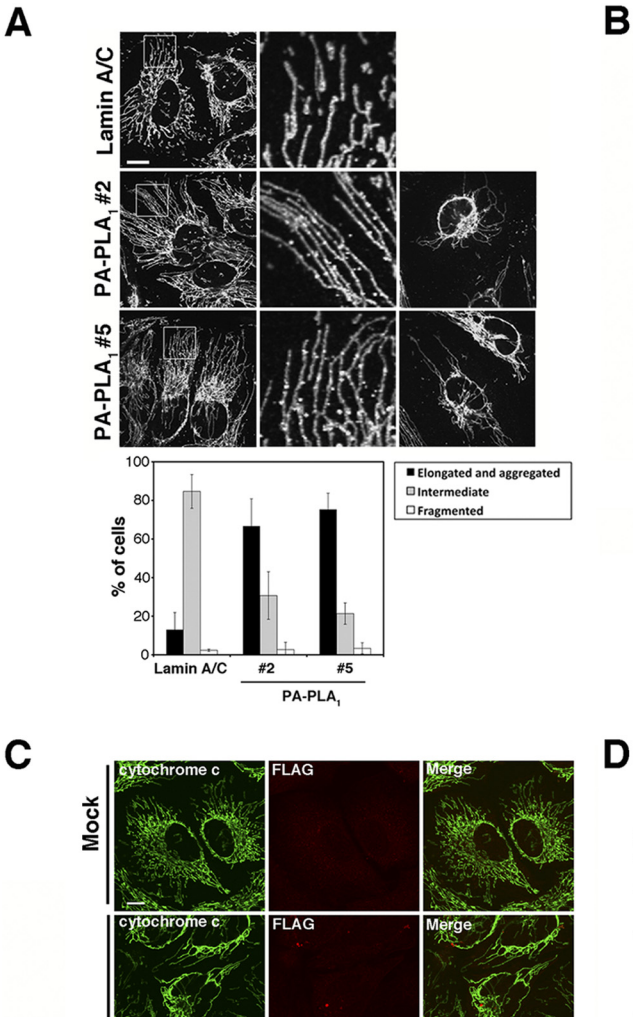
A
Lamin A/C
PA-PLA$_1$ #2
PA-PLA$_1$ #5
Elongated and aggregated
Intermediate
Fragmented
% of cells
Lamin A/C
#2
#5
PA-PLA$_1$
B
Length of mitochondria (μm)
Lamin A/C
PA-PLA$_1$ #2
PA-PLA$_1$ #5
C
Mock
PA-PLA$_1$#5 siRNA
cytochrome c
FLAG
Merge
FLAG-PA-PLA$_1$R WT
FLAG-PA-PLA$_1$R S537A
Elongated and aggregated
Intermediate
Fragmented
% of cells
FLAG
FLAG-PA-PLA$_1$R WT
FLAG-PA-PLA$_1$R S537A
Mock
PA-PLA$_1$ #5 siRNA
D
CCCP
Lamin A/C
PA-PLA$_1$#2
PA-PLA$_1$#5

PLA$_1$ siRNA5 (*bottom row*). Upon knockdown of PA-PLA$_1$, the percentage of cells with elongated or aggregated mitochondria was increased from about 10 to about 70% (Fig. 2*A*, *bottom graph*). The length of mitochondria in peripheral regions was increased 2.4-fold in cells transfected with PA-PLA$_1$ siRNA (Fig. 2*B*). Mitochondrial elongation observed upon PA-PLA$_1$ knockdown was significantly reversed by expression of siRNA-resistant PA-PLA$_1$ but not siRNA-resistant S537A mutant (Fig. 2*C*).

Mitochondrial elongation, interconnection, and aggregation can occur when mitochondrial fusion is promoted or fission is inhibited (25–27). To further verify the effects of the depletion of PA-PLA$_1$, HeLa cells were treated with CCCP. It has been reported that CCCP causes mitochondrial fragmentation in a Drp1-dependent manner (25). When PA-PLA$_1$ siRNA2- or siRNA5-transfected cells were treated with CCCP, much less fragmentation of mitochondria was detected (Fig. 2*D*, *middle* and *bottom rows*) compared with control (Lamin A/C siRNA-treated) cells (*top row*). These results indicate that the overexpression and depletion of PA-PLA$_1$ cause the fragmentation and elongation of mitochondria, respectively. Note that these effects depend on PA-PLA$_1$ activity.

PA-PLA$_1$ Counteracts the Action of MitoPLD on Mitochondria—MitoPLD is a mitochondrial surface PLD that produces PA via hydrolysis of cardiolipin (8). Overexpression of MitoPLD results in mitochondrial aggregation caused by the promotion of fusion events, whereas its siRNA-mediated knockdown results in mitochondrial fragmentation (8). Because PA-PLA$_1$ is a cytosolic protein and shows phospholipase A$_1$ activity against PA *in vitro* (12, 15, 23), it is plausible that PA-PLA$_1$ hydrolyzes mitochondrial surface PA, thereby regulating mitochondrial morphology. To test this idea, we first analyzed the effects of coexpression of MitoPLD and PA-PLA$_1$ on mitochondrial morphology (Fig. 3*A*). As reported previously (8), mitochondria became aggregated in the perinuclear region of MitoPLD-overexpressing cells (Fig. 3*A*, *top row*). When PA-PLA$_1$ was coexpressed with MitoPLD, the mitochondrial aggregation was prevented, and mitochondria spread throughout the cell (*middle row*). The expression of the S537A mutant had no effect (*bottom row*). Quantitative data (Fig. 3*A*, *graph*) support this viewpoint. Western blotting showed that the expression level of MitoPLD was not affected by coexpression with PA-PLA$_1$ or the S537A mutant (data not shown).

We next examined the effect of the expression of PA-PLA$_1$ on mitochondrial surface PA. Raf1-PABD-EGFP is a fluorescent sensor for PA (28) and has been successfully used to detect mitochondrial surface PA generated by MitoPLD (9). When expressed alone, Raf1-PABD-EGFP was localized in the cytosol in many cells (Fig. 3*B*, *top row*) but targeted to mitochondria in 28% of Raf1-PABD-EGFP-expressing cells (Fig. 3*B*, *graph*). The association of Raf1-PABD-EGFP with mitochondria may be in part due to the hydrophobic nature of Raf1-PABD. Upon coexpression with MitoPLD, Raf1-PABD-EGFP was redistributed from the cytosol to mitochondria (Fig. 3*B*, *third row*), and the percentage of cells with Raf1-PABD-EGFP on mitochondria increased to 53%. The binding of Raf1-PABD-EGFP to mitochondria did not significantly increase when a phospholipase D activity-defective mutant (MitoPLD H156N) was expressed (*fourth row*) or when a Raf1-PABD mutant that lacks PA binding activity (9) was coexpressed with MitoPLD (*fifth row*). These results demonstrate the specificity of this fluorescent probe. When PA-PLA$_1$ was coexpressed with Mito-PLD, the targeting of Raf1-PABD-EGFP to mitochondria decreased to the background level (*second row* from *bottom*). In contrast, the PA-PLA$_1$ S537A mutant did not affect the targeting of Raf1-PABD-EGFP to mitochondria (*bottom row*). The targeting of MitoPLD to mitochondria occurred regardless of whether the expressed PA-PLA$_1$ construct was the wild type (Fig. 3*B*, *second column* from *left*, *second* from the *bottom row*) or the mutant (*bottom row*), ruling out the possibility that the expression of PA-PLA$_1$ prevents the attachment of MitoPLD to mitochondria. The expression of PA-PLA$_1$ alone did not affect the localization of Raf1-PABD-EGFP (*second row*). Western blotting showed that the expression levels of MitoPLD and Raf1-PABD-EGFP were not affected by coexpression of PA-PLA$_1$ or the S537A mutant (data not shown). These results suggest that PA-PLA$_1$ cleaved PA produced by MitoPLD on the mitochondrial surface. Next, we measured mitochondrial PA and LPA by mass spectrometry. Mitochondrial fractions were prepared from control cells, MitoPLD-overexpressing cells, and PA-PLA$_1$-overexpressing cells. LC-electrospray ionization-MS/MS analysis was performed as described under "Experimental Procedures." As shown in Fig. 3*C*, no apparent differences in the content and composition of PA and LPA were observed among the mitochondrial fractions prepared from control, MitoPLD-, and PA-PLA$_1$-overexpressing cells. These results indicate that the total PA content of mitochondria was not drastically changed upon the overexpression of either MitoPLD or PA-PLA$_1$. Mitochondrial fission is regulated by Drp1, and the fusion is regulated by Mfn1/2 (6). To examine whether or not

FIGURE 2. **Knockdown of PA-PLA$_1$ induces elongation of mitochondria.** *A*, HeLa cells were treated with the indicated siRNAs for 72 h and subsequently stained with an antibody against Tom20. Higher magnification views of the *boxed* areas are shown on the *right* (*middle column*). *Scale bar*, 10 μm. Cells were classified according to their mitochondrial morphology: intermediate (mitochondria with tubular structures, which were dominantly observed in control (Lamin A/C-treated) cells (*top row*, *left column*)), elongated (most mitochondria were elongated (*middle* and *bottom rows*, *left column*) and aggregated (most mitochondria were aggregated near the nucleus with long tubule extensions to the cell periphery (*middle* and *bottom rows*, *right column*)), and fragmented (most mitochondria were fragmented, and filamentous mitochondria were scarcely found). The *bottom graph* shows the percentages of cells with the indicated mitochondrial morphologies. *Black*, *gray*, and *white bars* indicate elongated and aggregated, intermediate, and fragmented morphologies, respectively. At least 100 cells were analyzed. Data represent the means ± S.D. for three independent experiments. *B*, HeLa cells were treated with the indicated siRNAs and stained as in *A*. The mitochondrial length in the peripheral regions was analyzed as described under "Experimental Procedures". Twenty randomly selected cells were analyzed for each sample. Data represent the means ± S.D. for three independent experiments. *C*, HeLa cells were treated with PA-PLA$_1$5 siRNA or mock-treated for 48 h and then transfected with the indicated plasmids. At 24 h after transfection with the plasmid, the cells were fixed and stained with antibodies against cytochrome *c* and FLAG. *Scale bar*, 10 μm. The *bottom graph* shows the percentages of cells with the indicated mitochondrial morphologies. *Black*, *gray*, and *white bars* indicate elongated and aggregated, intermediate, and fragmented morphologies, respectively. At least 100 cells were analyzed for each sample. Data represent the means ± S.D. for three independent experiments. *, $p < 0.05$, Student's *t* test. *D*, HeLa cells were treated with the indicated siRNAs as in *A* and stained after incubation with 10 μM CCCP for 90 min. *Scale bar*, 10 μm. *Error bars* represent S.D.

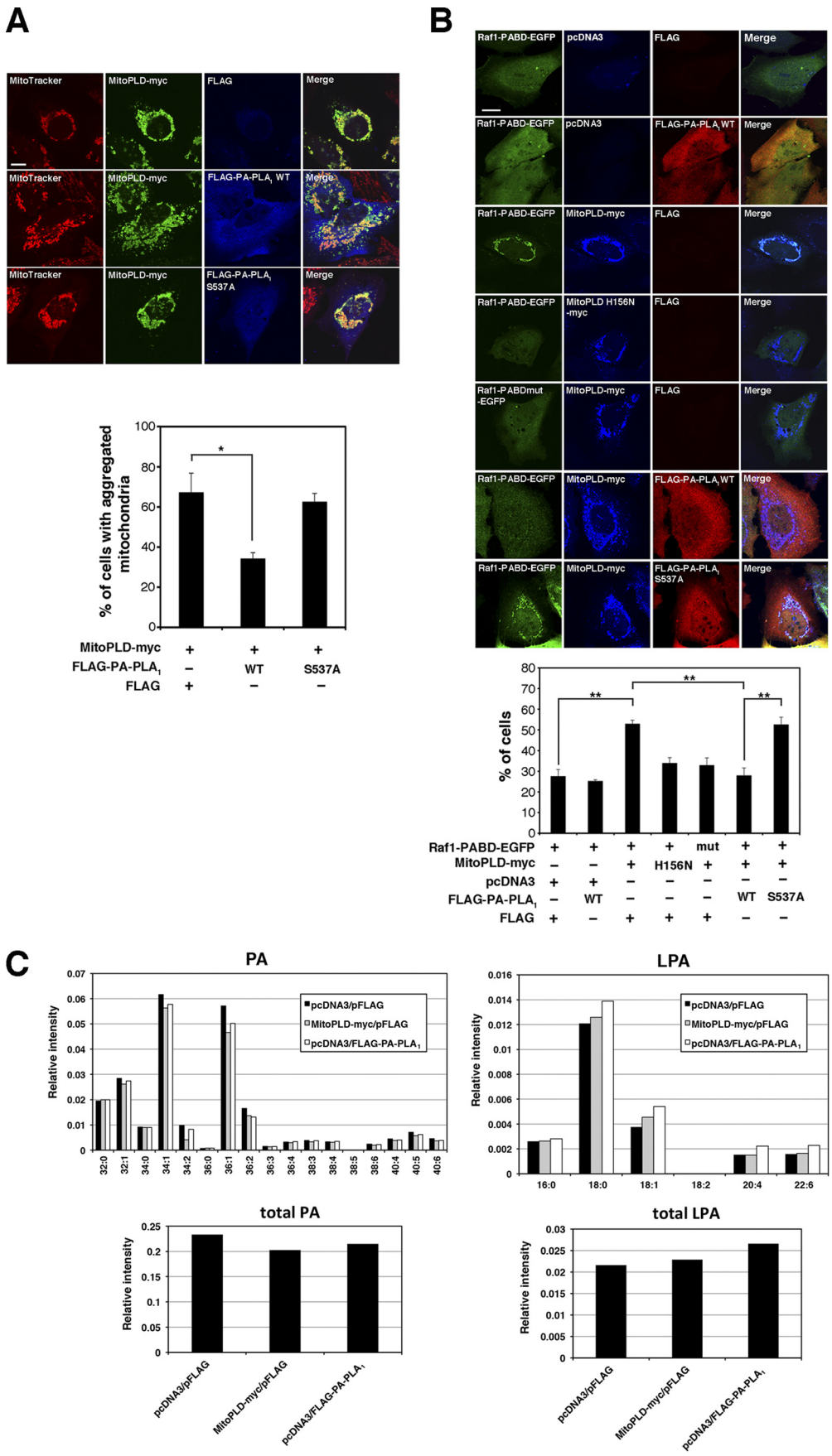
A
MitoTracker
MitoPLD-myc
FLAG
Merge
FLAG-PA-PLA1 WT
FLAG-PA-PLA1 S537A
% of cells with aggregated mitochondria
MitoPLD-myc
FLAG-PA-PLA1
FLAG
WT
S537A
B
Raf1-PABD-EGFP
pcDNA3
FLAG-PA-PLA1 WT
MitoPLD H156N -myc
Raf1-PABDmut -EGFP
% of cells
Raf1-PABD-EGFP
MitoPLD-myc
pcDNA3
FLAG-PA-PLA1
mut
H156N
WT
S537A
C
PA
LPA
Relative intensity
pcDNA3/pFLAG
MitoPLD-myc/pFLAG
pcDNA3/FLAG-PA-PLA1
total PA
total LPA

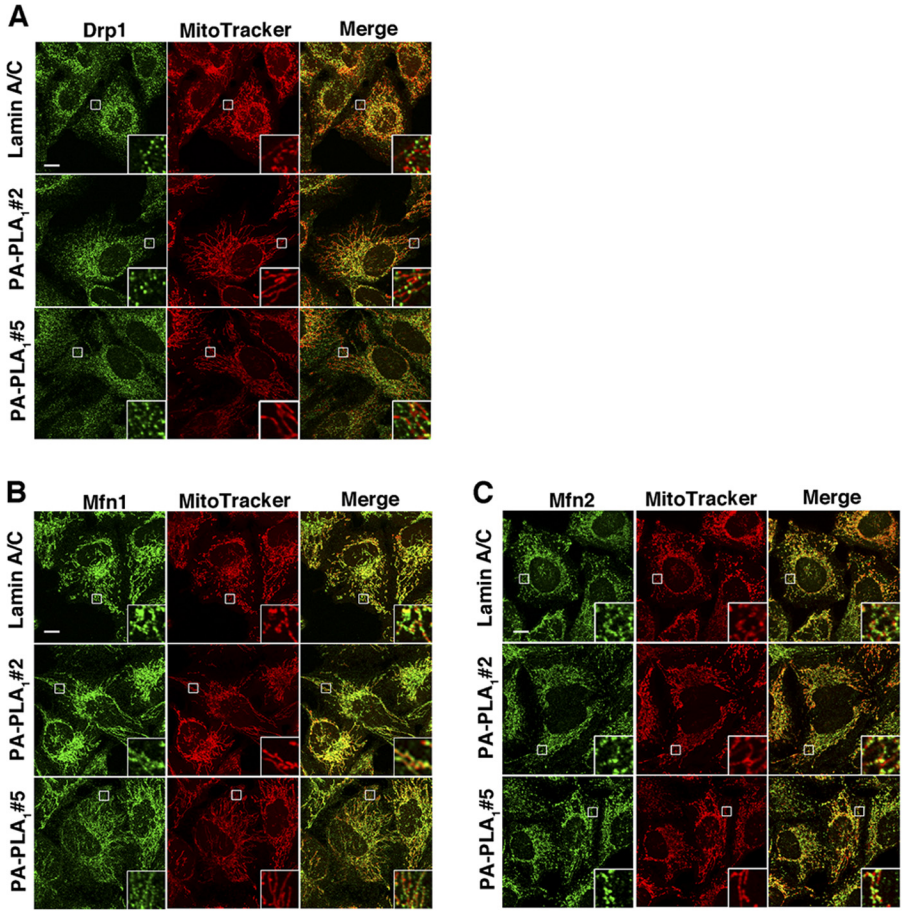

FIGURE 4. **Distributions of Drp1 and Mfn1/2 are not affected by depletion of PA-PLA$_1$.** HeLa cells were treated with the indicated siRNAs for 72 h and then double stained with an antibody against Drp1 (*A*), Mfn1 (*B*), or Mfn2 (*C*) and MitoTracker Red CMXRos. *Insets* are enlarged images of the *boxed* areas. *Scale bar*, 10 μm.

PA-PLA$_1$ directly affects the distribution of these GTPases, PA-PLA$_1$ was knocked down. As shown in Fig. 4*A*, treatment of cells with PA-PLA$_1$ siRNA2 (*middle panel*) or PA-PLA$_1$ siRNA5 (*bottom panel*) did not affect the distribution of Drp1. The enlarged images show that Drp1 was localized in constricted regions of elongated mitochondria (*middle* and *bottom panels*, *insets*). The PA-PLA$_1$ depletion also did not affect the distribution of Mfn1 (Fig. 4*B*) or Mfn2 (Fig. 4*C*). Likewise, overexpression of PA-PLA$_1$ caused little change in the distributions of these fission and fusion GTPases on mitochondria (data not shown).

Male PA-PLA$_1^{-/-}$ Mice Are Subfertile—To elucidate the *in vivo* function of PA-PLA$_1$, *PA-PLA$_1^{-/-}$* mice were generated (Fig. 5). The targeting vector was designed to contain exon 8 flanked by two *loxP* sites. It also contained a splicing acceptor and a geo marker (a fusion between the β-galactosidase and neomycin resistance genes) between exons 7 and 8 of the mouse *PA-PLA$_1$* gene (Fig. 5*A*). Chimeric mice were obtained by the conventional method, and the male chimeric mice were mated with female wild-type C57BL/6J mice to obtain *PA-PLA$_1^{+/geo}$* offspring. Southern blotting verified insertion of the geo marker (Fig. 5*B*). Homozygous *PA-PLA$_1^{geo/geo}$* mice were obtained by intercrossing heterozygous mice. *PA-PLA$_1^{geo/geo}$* mice showed no significant defects. A slight reduction in fertility was observed in males, but it was not significant (Fig. 5*E*).

FIGURE 3. **The ectopic expression of PA-PLA$_1$ counteracts that of MitoPLD.** *A*, HeLa cells were double transfected with the following plasmid/construct combinations: MitoPLD-myc and FLAG (*top row*), MitoPLD-myc and FLAG-PA-PLA$_1$ (*middle row*), and MitoPLD-myc and FLAG-PA-PLA$_1$ S537A mutant (*bottom row*). At 24 h after transfection, the cells were stained with MitoTracker Red CMXRos and antibodies against FLAG and myc. Representative images are shown. *Scale bar*, 10 μm. The *graph* shows the percentages of cells exhibiting perinuclear aggregation of mitochondria. At least 100 cells were evaluated for each sample. Data represent the means ± S.D. for three independent experiments. *, $p < 0.05$, Student's *t* test. *B*, HeLa cells were triple transfected with the following plasmid/construct combinations: Raf1-PABD-EGFP, pcDNA3, and FLAG (*top row*); Raf1-PABD-EGFP, pcDNA3, and FLAG-PA-PLA$_1$ (*second row*); Raf1-PABD-EGFP, MitoPLD-myc, and FLAG (*third row*); Raf1-PABD-EGFP, MitoPLD H156N-myc, and FLAG (*fourth row*); Raf1-PABD mutant (*mut*)-EGFP, MitoPLD-myc, and FLAG (*fifth row*); Raf1-PABD-EGFP, MitoPLD-myc, and FLAG-PA-PLA$_1$ (*sixth row*); and Raf1-PABD-EGFP, MitoPLD-myc, and FLAG-PA-PLA$_1$ S537A mutant (*bottom row*). At 24 h after transfection, the cells were stained with antibodies against FLAG and myc. Representative images are shown. For cells expressing Raf1-PABD-EGFP, MitoPLD-myc, and FLAG (*third row*) or Raf1-PABD-EGFP, MitoPLD-myc, and FLAG-PA-PLA$_1$ S537A mutant (*bottom row*), staining patterns of cells in which Raf1-PABD-EGFP is localized to mitochondria are presented. *Scale bar*, 10 μm. Cells with Raf1-PABD-EGFP on mitochondria were counted, and the quantitative data are shown. At least 100 cells were evaluated for each sample. Data represent the means ± S.D. for three independent experiments. **, $p < 0.01$, Student's *t* test. *C*, quantification of PA and LPA contents by mass spectrometry. HeLa cells were double transfected with the empty FLAG plasmid and pcDNA3, the empty FLAG plasmid and the plasmid encoding MitoPLD-myc, or the plasmid encoding FLAG-PA-PLA$_1$ and pcDNA3. At 24 h after transfection, cells were collected. PA and LPA contents of mitochondrial fractions were measured by mass spectrometry as described under "Experimental Procedures." Data represent relative intensities normalized by protein amount. The averages of two independent experiments are shown. *Error bars* represent S.D.

We noticed that *PA-PLA$_1$*$^{geo/geo}$ mice express a tiny amount of PA-PLA$_1$ protein (Fig. 5*D*). To completely delete the *PA-PLA$_1$* gene, *PA-PLA$_1$*$^{+/geo}$ mice were crossed with transgenic mice expressing Cre recombinase. Heterozygous mice (*PA-PLA$_1$*$^{+/-}$) were intercrossed to obtain *PA-PLA$_1$*$^{-/-}$ mice. Southern blotting verified the loss of exon 8 (Fig. 5*C*). Western blotting demonstrated a complete loss of PA-PLA$_1$ protein expression (Fig. 5*D*). *PA-PLA$_1$*$^{-/-}$ mice were apparently normal. However, *PA-PLA$_1$*$^{-/-}$ male mice were found to be subfertile (Fig. 5*E*). The number of sperm (Fig. 5*F*, *left graph*), testis weight (Fig. 5*F*, *right graph*), and germ cell arrangement in seminiferous tubules (Fig. 5*G*) were almost normal in *PA-PLA$_1$*$^{-/-}$ mice.

PA-PLA$_1$ Is Required for Sperm Tail Formation—We then analyzed spermatozoa collected from the cauda epididymis by

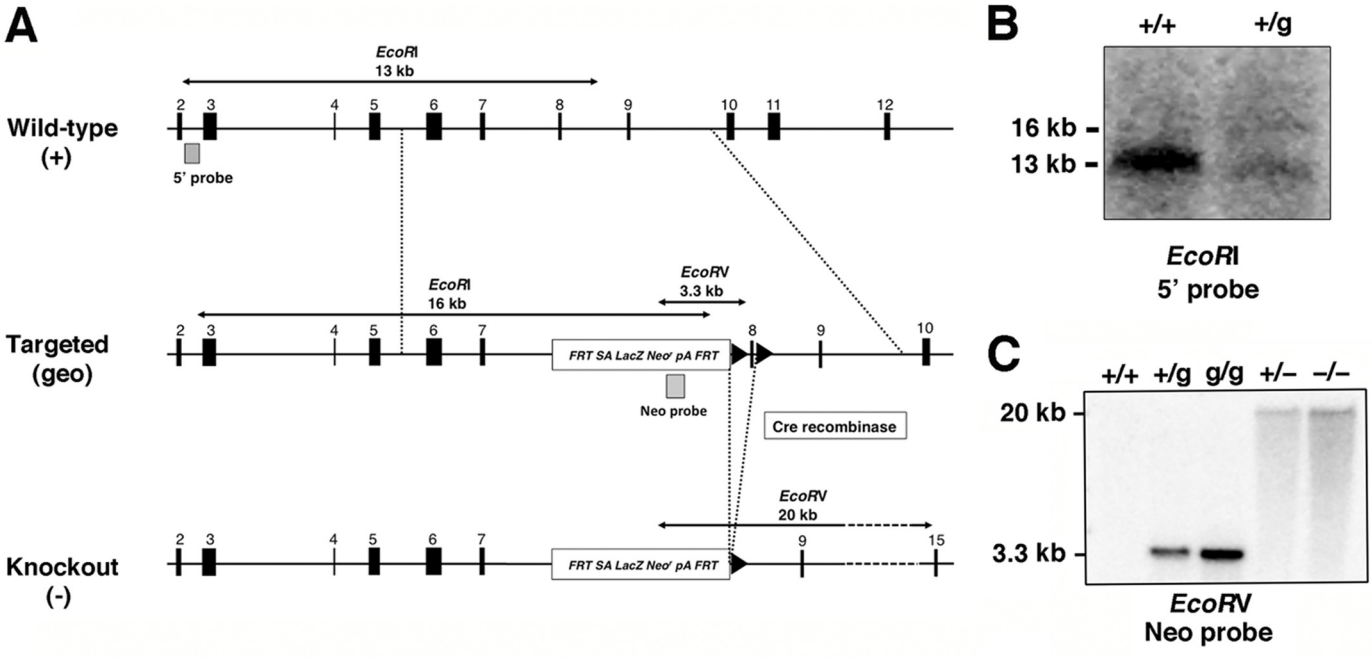

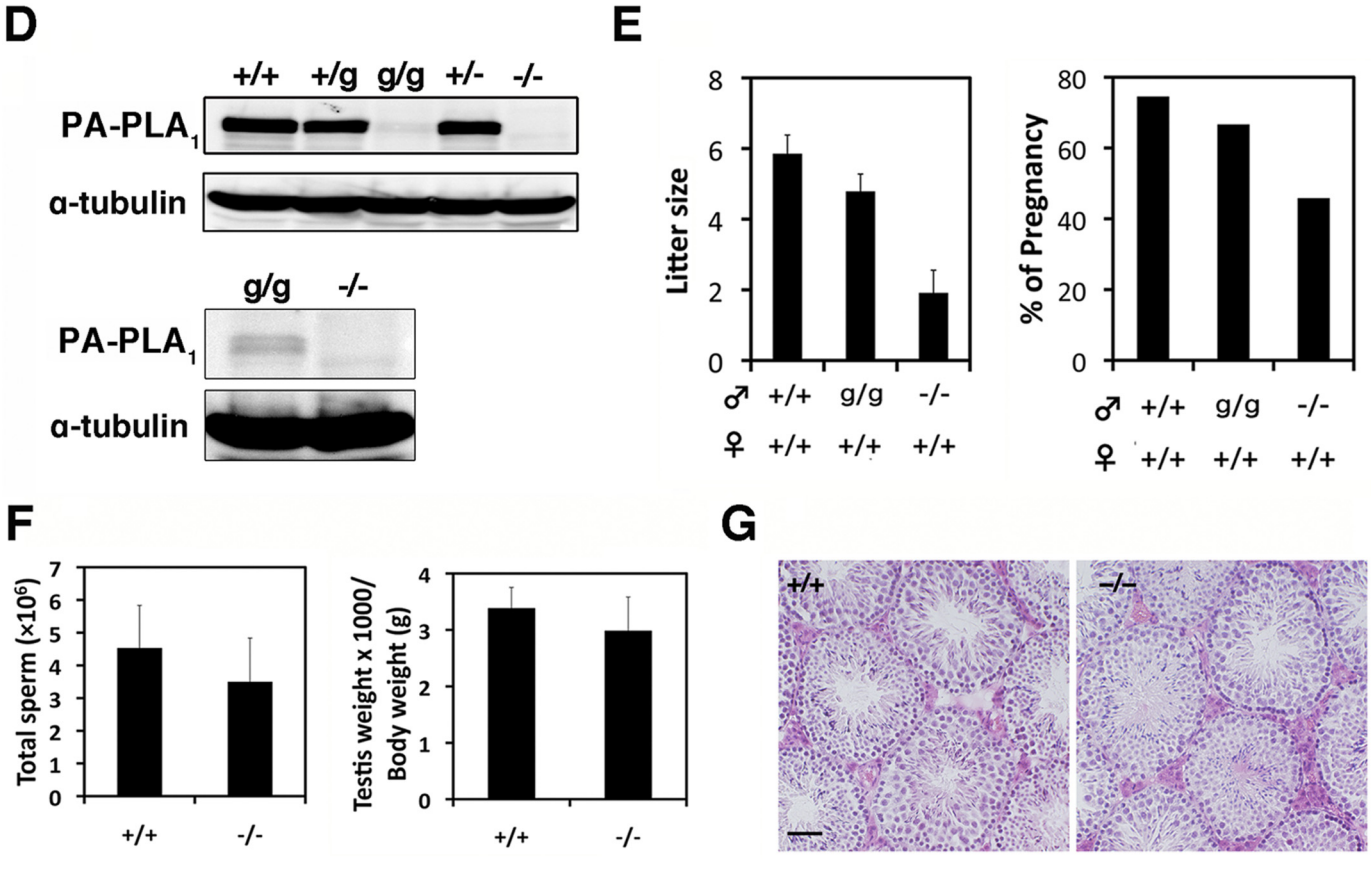

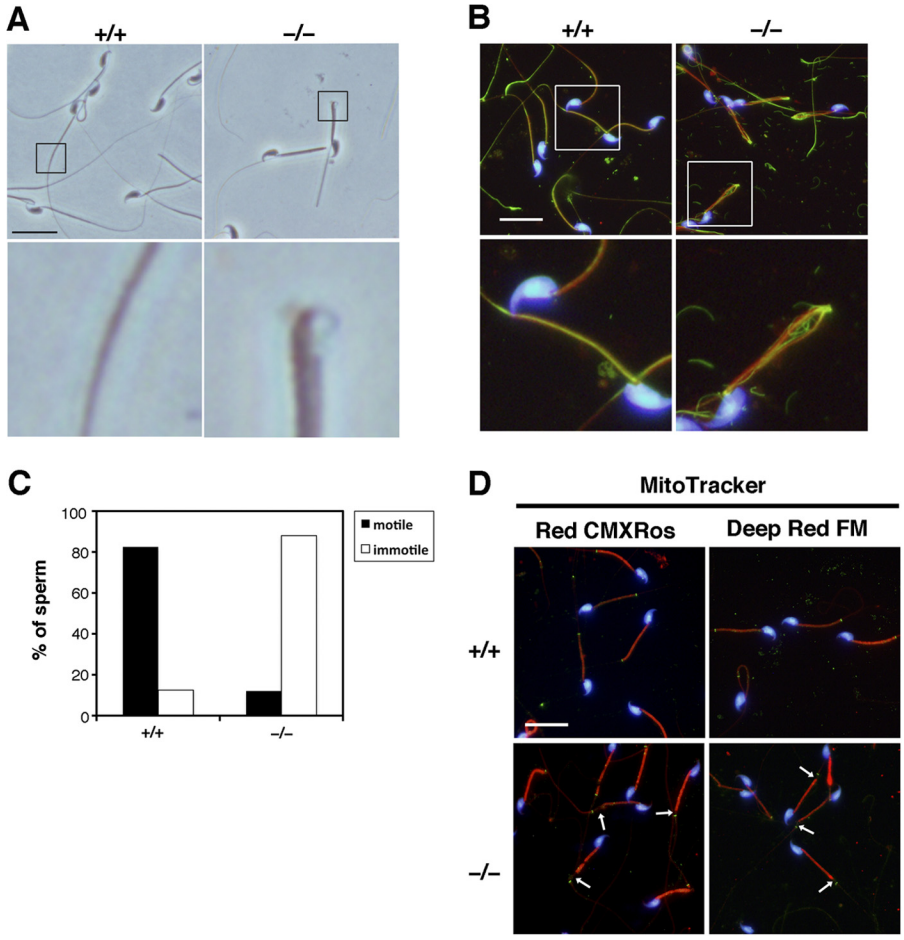

FIGURE 6. **Spermatozoa from *PA-PLA$_1^{-/-}$* mice are bent at the junction of the middle and principal pieces.** *A*, differential interference contrast images of spermatozoa derived from the cauda epididymis of *PA-PLA$_1^{+/+}$* and *PA-PLA$_1^{-/-}$* mice. The *lower row* shows enlarged images of the *boxed* areas in the *upper row*. *Scale bar*, 20 μm. *B*, spermatozoa from the cauda epididymis of *PA-PLA$_1^{+/+}$* and *PA-PLA$_1^{-/-}$* mice were triple stained with Hoechst 33342 (*blue*), MitoTracker Red CMXRos (*red*), and anti-α-tubulin antibody (*green*). The *lower row* shows enlarged images of the *boxed* areas in the *upper row*. *Scale bar*, 20 μm. *C*, motility of spermatozoa derived from the cauda epididymis was recorded for 10 s. At least 100 spermatozoa were assessed. The data are the averages for two independent experiments. *D*, spermatozoa collected from the cauda epididymis of *PA-PLA$_1^{+/+}$* and *PA-PLA$_1^{-/-}$* mice were triple stained with Hoechst 33342 (*blue*), anti-SEPT4 antibody (*green*), and mitochondrial membrane potential-sensitive dye MitoTracker Red CMXRos or mitochondrial membrane potential-insensitive dye MitoTracker Deep Red FM (*red*). *Arrows* indicate the sites where the MitoTracker staining was absent. *Scale bar*, 20 μm.

differential interference contrast microscopy. Strikingly, spermatozoa from *PA-PLA$_1^{-/-}$* mice were sharply bent between the middle and principal pieces, exhibiting a hairpin-like structure (Fig. 6*A*). Microtubules were disrupted at that position (Fig. 6*B*), and about 90% of the spermatozoa from *PA-PLA$_1^{-/-}$* mice exhibited impaired movement (Fig. 6*C*). It has been reported that a defect in the annulus, a fibrous ring structure connecting the middle and principal pieces of the mammalian sperm flagellum (30), causes the structure to be bent between the middle and principal pieces (19). Staining with an antibody against SEPT4, a main structural component of the annulus (19), revealed that spermatozoa from *PA-PLA$_1^{-/-}$* mice possessed an annulus that was not attached to the mitochondrial sheath, whereas that in control mice was attached. A small gap structure, which was not stained with MitoTracker, was present between the mitochondrial sheath and the annulus in spermatozoa from *PA-PLA$_1^{-/-}$* mice (Fig. 6*D*, *arrows*).

FIGURE 5. **Subfertility of male *PA-PLA$_1^{-/-}$* mice.** *A*, schematic representation of the wild-type (+), targeted (geo), and knock-out (−) alleles. The lipase consensus sequence SHSLG is encoded in exon 10. Cre-mediated deletion of exon 8 is supposed to cause a frameshift. Exons of the *PA-PLA$_1$* gene and *loxP* sequences are indicated by *black boxes* and *closed triangles*, respectively. *FRT*, Flp recombination target; *SA*, splice acceptor sequence of mouse engrailed 2; *LacZ*, β-galactosidase gene; *Neo^r*, neomycin resistance gene; *pA*, SV40 polyadenylation signal. *B*, Southern blot analysis of EcoRI-digested genomic DNA derived from the wild-type allele (+/+) and heterozygous targeted allele (+/geo). The 5′ probe in *A* recognized 13- and 16-kb fragments of the wild-type and targeted alleles, respectively. *g* denotes geo. *C*, Southern blot analysis of EcoRV-digested genomic DNA from the wild-type (+/+), heterozygous targeted (+/geo), homozygous targeted (geo/geo), heterozygous (+/−), and knock-out (−/−) alleles. The *Neo* probe in *A* recognized 3.3- and 20-kb fragments of the targeted and knock-out alleles, respectively. *D*, testis lysates (100 μg) were analyzed by Western blotting with a monoclonal antibody against PA-PLA$_1$ and an anti-α-tubulin antibody. The *bottom panel* shows a longer exposure image. *E*, average litter size and pregnancy rate of *PA-PLA$_1^{-/-}$* mice. The numbers of matings were 55, 66, and 24 for male +/+, g/g, and −/−, respectively. ♀, female. The average litter sizes were calculated as the number of pups per number of matings. *Error bars* represent the S.E. for each set of crossing experiments. *F*, the average number of spermatozoa collected from the cauda epididymis. Data are means ± S.E. (+/+, $n = 11$; −/−, $n = 10$) (*left graph*). Testis weight was normalized as to body weight. Data are means ± S.E. (+/+, $n = 9$; −/−, $n = 9$) (*right graph*). *G*, H&E staining of seminiferous tubules of testes from *PA-PLA$_1^{+/+}$* and *PA-PLA$_1^{-/-}$* mice. *Scale bar*, 40 μm.

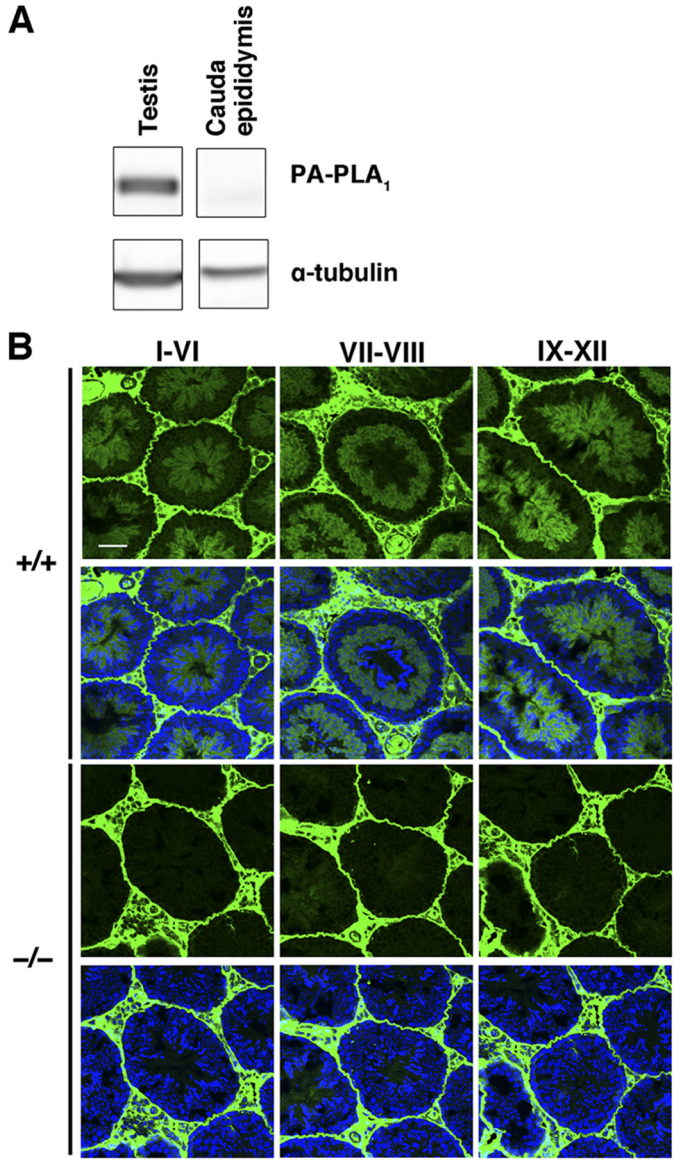

FIGURE 7. **Stage-specific expression of PA-PLA$_1$ during spermatogenesis.** *A*, total protein lysates (50 μg) of testis and cauda epididymis were analyzed by Western blotting. *B*, testis sections from *PA-PLA$_1^{+/+}$* and *PA-PLA$_1^{-/-}$* mice were double stained with a monoclonal antibody against PA-PLA$_1$ (*green*) and Hoechst 33342 (*blue*). Staining patterns of stages I–VI, VII-VIII, and IX–XII of the seminiferous epithelium cycle are shown. The intense staining between seminiferous tubules is due to nonspecific binding of secondary antibody. No staining was observed in *PA-PLA$_1^{-/-}$* cross-sections (*third row*), indicating the specificity of the antibody. *Scale bars*, 40 μm.

PA-PLA$_1$ Is Involved in the Organization of Mitochondria during Spermiogenesis—To elucidate how loss of *PA-PLA$_1$* causes the abnormal structure comprising a bent sperm flagellum, we first examined at which stage PA-PLA$_1$ is expressed during spermatogenesis. The PA-PLA$_1$ protein was detected in testicular cells but not in the cauda epididymis containing mature sperm (Fig. 7*A*). The expression of PA-PLA$_1$ was further examined by immunostaining of cross-sections of seminiferous tubules with a monoclonal antibody against PA-PLA$_1$. Results showed that PA-PLA$_1$ protein was expressed in round and elongating spermatids but not in spermatocytes or spermatogonia (Fig. 7*B*, *top row*). Relatively strong staining was observed at stages IX–XII of the cycle of seminiferous epithelium (31), which contained elongating spermatids (steps 9–12).

Spermatozoa formed in the testis enter the caput epididymis and then migrate to the cauda region where they are stored. To clarify when the hairpin-like structure is created, we compared the shapes of spermatozoa collected from the testis, caput epididymis, and cauda epididymis of *PA-PLA$_1^{-/-}$* mice. As shown in Fig. 8*A*, the ratio of spermatozoa with the hairpin-like structure increased as sperm migrated from the testis to the cauda region. The ratio of spermatozoa with an abnormal microtubule structure increased similarly (Fig. 8*B*). Most of the spermatozoa from *PA-PLA$_1^{-/-}$* testis and caput epididymis were found to have a straight junction between the middle and principal pieces (Fig. 8*A*). In these spermatozoa, a narrow segment adjacent to the mitochondrial sheath was observed, and the mitochondrial sheath and principal piece were separated by this short region (Fig. 8*A*, *enlarged image*, *arrowheads*). This narrow segment corresponds to the gap structure between the mitochondrial sheath and the annulus (Fig. 6*D*, *arrows*). As shown in Fig. 8*C*, the lengths of the mitochondrial sheaths of spermatozoa prepared from testis, caput epididymis, and cauda epididymis of *PA-PLA$_1^{-/-}$* mice were almost identical but were shorter than those in *PA-PLA$_1^{+/+}$* mice. These results suggest that the shortened mitochondrial sheath is the cause of the gap structure between the middle and principal pieces.

The sperm defects found in *PA-PLA$_1^{-/-}$* mice are quite similar to those recently reported in mitochondrial glutathione peroxidase 4 (*mGPx4*) knock-out mice (32, 33). *mGPx4* is a structural component of the sperm mitochondria capsule. Spermatozoa of *mGPx4* knock-out mice have a truncated mitochondrial sheath, and their mitochondrial structure is irregular and swollen. To examine the structure of mitochondria in spermatozoa from *PA-PLA$_1^{-/-}$* mice, electron microscopy was performed. Results showed that mitochondria in spermatozoa from *PA-PLA$_1^{-/-}$* mice are irregular and aligned in a disorganized manner (Fig. 8*D*). Overall, it is most likely that spermatozoa produced in *PA-PLA$_1^{-/-}$* mice testes possess a disorganized mitochondrial sheath. Because of the absence of rigid connection between the middle and principal pieces, *PA-PLA$_1$*-deficient spermatozoa may become bent during their migration to the cauda epididymis and/or when their flagella start moving in the cauda epididymis. These results suggest the importance of PA-PLA$_1$ in the mitochondrial organization during spermiogenesis.

KIAA0725p Is Involved in the Mitochondrial Dynamics in MEFs—We examined whether mitochondrial morphology is also affected in MEFs derived from *PA-PLA$_1^{-/-}$* mice. In contrast to spermatids, no apparent morphological change in mitochondria was observed (Fig. 9).

KIAA0725p is a member of the iPLA$_1$ family and, like PA-PLA$_1$, shows phospholipase A$_1$ activity against PA *in vitro* (13, 23). KIAA0725p is expressed broadly in many tissues (13). To test the possibility that KIAA0725p is also involved in mitochondrial dynamics, KIAA0725p was knocked down in HeLa cells (Fig. 10*A*). Differing from the case of PA-PLA$_1$, siRNA-mediated knockdown of KIAA0725p did not cause the elongation or aggregation of mitochondria. We showed previously that the subcellular localization of KIAA0725p is different

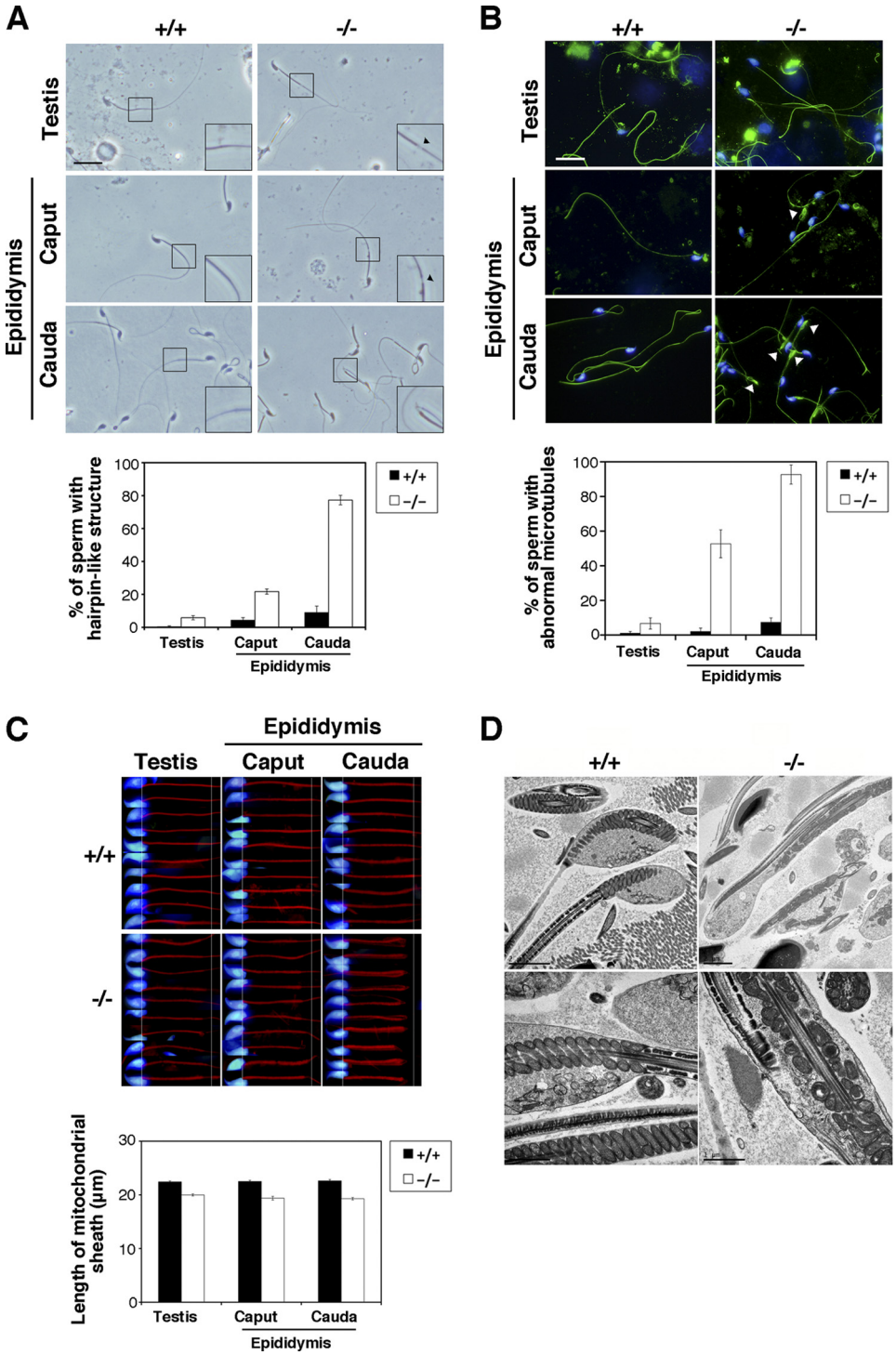

FIGURE 8. **PA-PLA$_1$ deficiency produces an abnormal mitochondrial sheath.** *A*, differential interference contrast images of spermatozoa derived from the testis (*top row*), caput epididymis (*middle row*), and cauda epididymis (*bottom row*) of *PA-PLA$_1^{+/+}$* and *PA-PLA$_1^{-/-}$* mice. *Insets* show enlarged images of the *boxed* areas. *Arrowheads* indicate the segment between the mitochondrial sheath and the principal piece. *Scale bar*, 20 μm. Quantitative data are shown at the *bottom*. At least 100 spermatozoa were counted for each sample. Data are means ± S.D. ($n = 3$). *B*, spermatozoa from *PA-PLA$_1^{+/+}$* and *PA-PLA$_1^{-/-}$* mice were double stained with Hoechst 33342 (*blue*) and anti-α-tubulin antibody (*green*). *Arrowheads* indicate an abnormal microtubule structure. *Scale bar*, 20 μm. Quantitative data are shown at the *bottom*. At least 100 spermatozoa were counted for each sample. Data are means ± S.D. ($n = 3$) *C*, spermatozoa from *PA-PLA$_1^{+/+}$* and *PA-PLA$_1^{-/-}$* mice were double stained with Hoechst 33342 (*blue*) and MitoTracker Red CMXRos (*red*). Images were captured with an Olympus DP70 charge-coupled device camera attached to an Olympus IX70 microscope, and the length of the mitochondrial sheath was determined using ImageJ software. Quantitative data are shown in the *bottom graph*. Three mice were analyzed for each genotype. For each mouse, 20 spermatozoa were analyzed. Data are means ± S.D. *D*, spermatozoa from the cauda epididymis of *PA-PLA$_1^{+/+}$* and *PA-PLA$_1^{-/-}$* mice were analyzed by electron microscopy. *Upper row scale bar*, 2 μm; *lower row scale bar*, 1 μm. *Error bars* represent S.D.

among cell lines (22). In HeLa cells, KIAA0725p is localized to the Golgi and the cytosol, whereas it is predominantly localized to the cytosol in MEFs. We next examined the effects of KIAA0725p depletion in MEFs. MEFs were treated with siRNAs targeting PA-PLA$_1$ or KIAA0725p, and then the morphology of mitochondria was examined (Fig. 10*B*). siRNA-

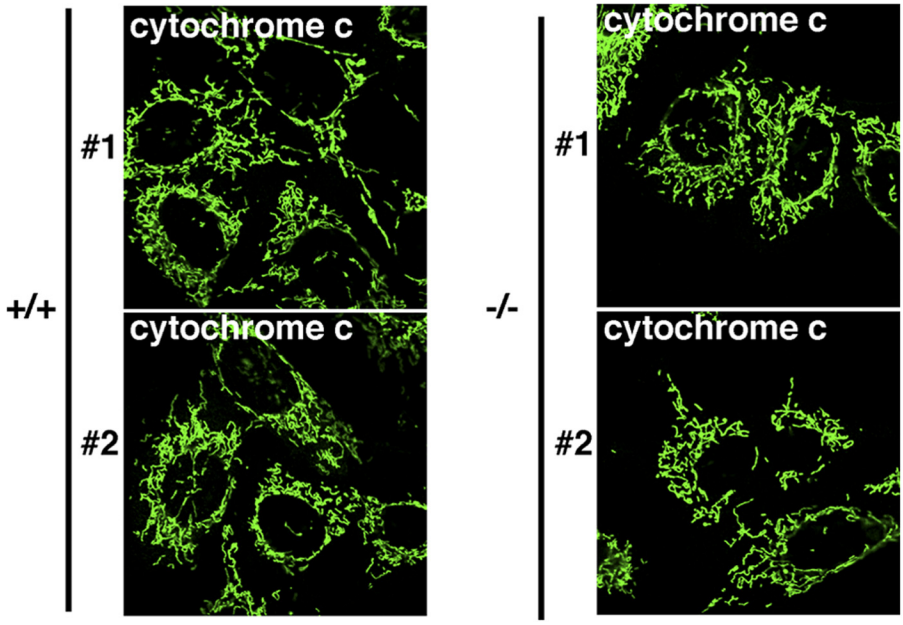

FIGURE 9. **Mitochondrial morphology in *PA-PLA$_1^{-/-}$* MEF cells.** MEFs isolated from *PA-PLA$_1^{+/+}$* and *PA-PLA$_1^{-/-}$* mice were stained with an antibody against cytochrome *c*. Two independent cell lines were analyzed for each genotype.

mediated knockdown of PA-PLA$_1$ did not cause significant changes in mitochondrial morphology in MEFs. Instead, elongation of mitochondrial tubules was observed in MEFs transfected with KIAA0725p siRNA1 (Fig. 10*B*, *fourth row*) and siRNA5 (*bottom row*). In some cells, interconnected mitochondrial aggregates were detected in the perinuclear region (Fig. 10*B*, *fourth* and *bottom rows*, *right column*). These results suggest that KIAA0725p is involved in the regulation of mitochondrial morphology in MEFs.

DISCUSSION

In this study, we demonstrated that PA-PLA$_1$ regulates mitochondrial morphology. A specific physiological role of PA-PLA$_1$ in mitochondrial function was verified in *PA-PLA$_1$*-deficient sperm.

It is a little surprising that PA-PLA$_1$ affects mitochondria. Because PA-PLA$_1$ is a cytosolic protein (15), it can affect all membranes in contact with the cytosol. We cannot exclude the possibility that other organelle membranes are also affected by PA-PLA$_1$, but our results suggest that mitochondria are one of the critical targets of PA-PLA$_1$. The phenotype of *PA-PLA$_1^{-/-}$* mice is quite similar to that of *mGPx4$^{-/-}$* mice (32, 33), supporting the idea that PA-PLA$_1$ affects mitochondria. Interestingly, the YOR022c protein, the sole iPLA$_1$ in *Saccharomyces cerevisiae*, was reported to be localized in mitochondria (34). A recent genome-wide interaction study showed that *YOR022c* genetically interacts with several genes implicated in mitochondrial dynamics and mitochondrial lipid metabolism. Examples of the genes include *UGO1*, an outer membrane component implicated in mitochondrial membrane fusion, and *UPS1*, a phosphatidic acid transfer protein in mitochondria (35).

PA-PLA$_1$ exhibits PLA$_1$ activity toward PA (12, 15, 23). The overexpression and depletion of PA-PLA$_1$ cause the fragmentation and elongation of mitochondria, respectively. MitoPLD has been postulated to facilitate Mfn-mediated mitochondrial fusion by producing PA from cardiolipin (8). Overexpression of PA-PLA$_1$ counteracts that of MitoPLD in terms of mitochondrial dynamics. These results encouraged us to propose a working model that PA-PLA$_1$ hydrolyzes mitochondrial surface PA and thereby regulates mitochondrial morphology. Our results using Raf1-PABD as a PA sensor support this model. However, lipid analysis by mass spectrometry failed to show significant changes in the PA content of mitochondria upon overexpression of MitoPLD or PA-PLA$_1$. It is possible that a small fraction of the total mitochondrial lipids might be metabolized by MitoPLD and PA-PLA$_1$. More sensitive and direct measurement of mitochondrial surface PA is necessary to further verify the model.

Drp1, which is essential for mitochondrial fission (6), was normally targeted to constricted regions of elongated mitochondria in PA-PLA$_1$-knocked down cells (Fig. 4*A*). Moreover, knockdown of PA-PLA$_1$ retarded CCCP-induced mitochondrial fragmentation (Fig. 2*C*). These results suggest that PA-PLA$_1$ knockdown does not affect the association of Drp1 with mitochondria but may inhibit the fission of constricted mitochondria. PA and LPA are cone- and inverted cone-shaped lipids that generate negative and positive curvature of membranes, respectively (3). The PA consumption and/or LPA production by PA-PLA$_1$ at mitochondrial constriction sites might be important for mitochondrial fission. The viewpoint that LPA favors the fission of mitochondria is consistent with our recent study, which demonstrated that CI-976, an inhibitor for lysophospholipid acyltransferases such as lysophosphatidic acid acyltransferase (3), causes mitochondrial fragmentation (22). However, given that mitochondrial morphology is regulated by the balance between fusion and fission, it is also possible that PA-PLA$_1$ negatively regulates Mfn-mediated fusion rather than stimulates mitochondrial fission. It has been reported that phospholipase D$_1$ acts on the mitochondrial sur-

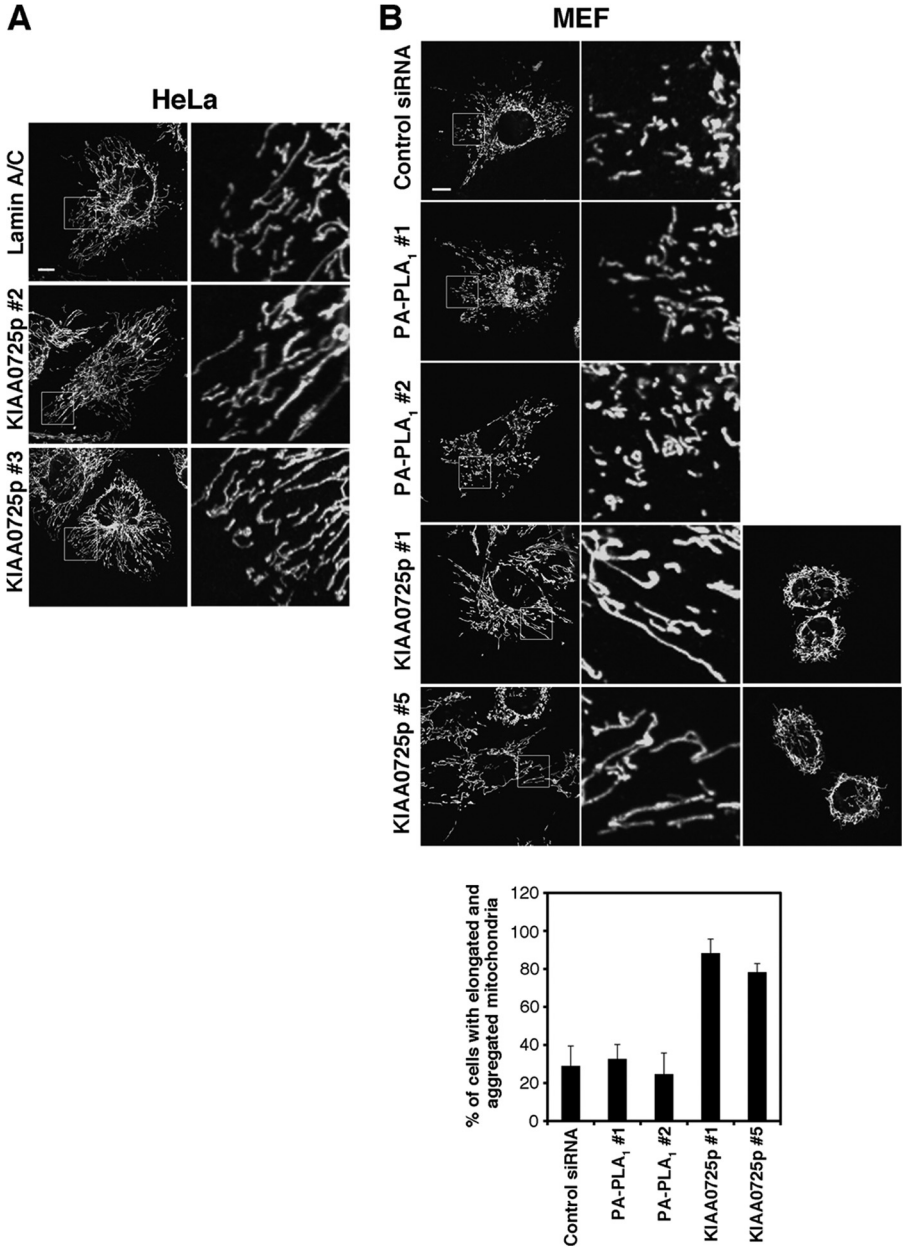

FIGURE 10. **KIAA0725p regulates mitochondrial dynamics in MEFs.** HeLa cells (*A*) or MEFs (*B*) were treated with the indicated siRNAs for 72 h and subsequently stained with an antibody against cytochrome *c*. Higher magnification views of the *boxed* areas are shown on the *right*. *Scale bar*, 10 μm. *B*, quantitative data are shown at the *bottom*. Cells in which most mitochondria were elongated or aggregated were counted. At least 100 cells were analyzed. Data represent the means $\pm$ S.D. for three independent experiments. *Error bars* represent S.D.

face (36, 37). In addition, PA can be generated by the phosphorylation of diacylglycerol and the acylation of LPA. It is possible that PA-PLA$_1$ metabolizes PA produced via several routes.

The results of knock-out mice studies suggest a possible functional link between PA-PLA$_1$ and Mito-PLD *in vivo*. Mito-PLD ablation causes meiotic arrest during spermatogenesis (9, 38). In MitoPLD-depleted cells, the formation of the nuage, a perinuclear structure involved in piRNA biogenesis/function (39), is impaired (9, 38). Huang *et al.* (9) have proposed that PA produced on the surface of mitochondria by MitoPLD recruits or activates nuage components. Consistent with this idea, expression of MitoPLD is high in spermatocytes undergoing meiosis and low in round spermatids. Meanwhile, PA-PLA$_1$ protein is expressed in round and elongating spermatids but not in spermatocytes. Because the nuage acts as intermitochondrial "cement" (39), it may prohibit the reorganization of mitochondria required for subsequent flagellum formation. As spermatogenesis progresses, PA-PLA$_1$ may metabolize PA and thus adjust the PA level for subsequent mitochondrial reorganization steps in spermatids. MitoPLD might be involved in the formation of piRNA in early stages of spermatogenesis and later in the regulation of mitochondrial morphology. Indeed, loss of MitoPLD affects the mitochondrial morphology in MEFs (9), suggesting that its role is not limited to piRNA generation. Huang *et al.* (9) have suggested that a PA phosphatase, Lipin 1, may metabolize PA produced by MitoPLD. The relationship between PA-PLA$_1$ and Lipin 1 in the regulation of mitochondrial dynamics should be clarified in the future. Mitochondria

align along a flagellum in late elongating spermatids, *e.g.* step 15 in mice. Prior to this alignment step, pronounced expression of the fusion and fission factors is observed in late round spermatids and early elongating spermatids (40, 41). One report suggested the necessity of intensive homogenization of mitochondria at a certain stage of spermiogenesis (*i.e.* steps 8–12) (41). It is plausible that PA-PLA$_1$ might be involved in the regulation of mitochondrial fusion and fission at this stage.

A remaining question concerning iPLA$_1$ in mammals concerns functional separation or redundancy between PA-PLA$_1$ and KIAA0725p. KIAA0725p exhibits an enzyme activity similar to that of PA-PLA$_1$ (13, 23). Recent reports have mentioned mutations of the *PA-PLA$_1$/DDHD1* gene (16) and *KIAA0725p/DDHD2* gene (42, 43) in hereditary spastic paraplegia patients, suggesting that the two proteins have similar physiological significance in the nervous system. Mutations in the Lipin 1 gene in mice (44, 45) and rats (46) induce hind limb paralysis, which is a typical symptom of hereditary spastic paraplegia. This suggests the importance of PA metabolism in these rodents. Although *PA-PLA$_1^{-/-}$* mice did not show significant gait disturbance, precise neurological examination will be necessary to determine the effect of *PA-PLA$_1$* gene deletion on the nervous system. Redundant functions between PA-PLA$_1$ and KIAA0725p may explain the fact that mitochondria in MEFs derived from *PA-PLA$_1^{-/-}$* mice show a normal morphology (Fig. 9). Consistent with this idea, KIAA0725p knockdown caused mitochondrial elongation in MEFs but not in HeLa cells (Fig. 10). KIAA0725p is predominantly localized to the cytosol in MEFs (22). Perhaps, cytosolic KIAA0725p can act on mitochondrial surface lipids in a manner similar to PA-PLA$_1$. The expression levels and cellular distribution of PA-PLA$_1$ and KIAA0725p may determine which protein mainly functions in each cellular process.

Acknowledgments—We thank Dr. Aizawa of the RIKEN Center for Developmental Biology for donation of the TT2 cells. We also thank Drs. Sekimizu and Hamamoto of the University of Tokyo for genetic manipulation of mice. We are also grateful to Dr. Tagaya of Tokyo University of Pharmacy and Life Sciences and Dr. Shishido for critical reading of the manuscript.

REFERENCES

1. Haucke, V., and Di Paolo, G. (2007) Lipids and lipid modifications in the regulation of membrane traffic. *Curr. Opin. Cell Biol.* **19,** 426–435
2. Wang, X., Devaiah, S. P., Zhang, W., and Welti, R. (2006) Signaling functions of phosphatidic acid. *Prog. Lipid Res.* **45,** 250–278
3. Ha, K. D., Clarke, B. A., and Brown, W. J. (2012) Regulation of the Golgi complex by phospholipid remodeling enzymes. *Biochim. Biophys. Acta* **1821,** 1078–1088
4. Han, G. S., and Carman, G. M. (2010) Characterization of the human LPIN1-encoded phosphatidate phosphatase isoforms. *J. Biol. Chem.* **285,** 14628–14638
5. Shindou, H., Hishikawa, D., Harayama, T., Eto, M., and Shimizu, T. (2013) Generation of membrane diversity by lysophospholipid acyltransferases. *J. Biochem.* **154,** 21–28
6. Youle, R. J., and van der Bliek, A. M. (2012) Mitochondrial fission, fusion, and stress. *Science* **337,** 1062–1065
7. Yang, C. Y., and Frohman, M. A. (2012) Mitochondria: Signaling with phosphatidic acid. *Int. J. Biochem. Cell Biol.* **44,** 1346–1350
8. Choi, S. Y., Huang, P., Jenkins, G. M., Chan, D. C., Schiller, J., and Frohman, M. A. (2006) A common lipid links Mfn-mediated mitochondrial fusion and SNARE-regulated exocytosis. *Nat. Cell Biol.* **8,** 1255–1262
9. Huang, H., Gao, Q., Peng, X., Choi, S. Y., Sarma, K., Ren, H., Morris, A. J., and Frohman, M. A. (2011) piRNA-associated germline nuage formation and spermatogenesis require MitoPLD profusogenic mitochondrial-surface lipid signaling. *Dev. Cell* **20,** 376–387
10. Muliyil, S., Krishnakumar, P., and Narasimha, M. (2011) Spatial, temporal and molecular hierarchies in the link between death, delamination and dorsal closure. *Development* **138,** 3043–3054
11. Tani, K., Kogure, T., and Inoue, H. (2013) Intracellular phospholipase A$_1$. *Biomol. Concepts* **3,** 471–478
12. Higgs, H. N., Han, M. H., Johnson, G. E., and Glomset, J. A. (1998) Cloning of a phosphatidic acid-preferring phospholipase A$_1$ from bovine testis. *J. Biol. Chem.* **273,** 5468–5477
13. Nakajima, K., Sonoda, H., Mizoguchi, T., Aoki, J., Arai, H., Nagahama, M., Tagaya, M., and Tani, K. (2002) A novel phospholipase A$_1$ with sequence homology to a mammalian Sec23p-interacting protein, p125. *J. Biol. Chem.* **277,** 11329–11335
14. Tani, K., Mizoguchi, T., Iwamatsu, A., Hatsuzawa, K., and Tagaya, M. (1999) p125 is a novel mammalian Sec23p-interacting protein with structural similarity to phospholipid-modifying proteins. *J. Biol. Chem.* **274,** 20505–20512
15. Higgs, H. N., and Glomset, J. A. (1994) Identification of a phosphatidic acid-preferring phospholipase A$_1$ from bovine brain and testis. *Proc. Natl. Acad. Sci. U.S.A.* **91,** 9574–9578
16. Tesson, C., Nawara, M., Salih, M. A., Rossignol, R., Zaki, M. S., Al Balwi, M., Schule, R., Mignot, C., Obre, E., Bouhouche, A., Santorelli, F. M., Durand, C. M., Oteyza, A. C., El-Hachimi, K. H., Al Drees, A., Bouslam, N., Lamari, F., Elmalik, S. A., Kabiraj, M. M., Seidahmed, M. Z., Esteves, T., Gaussen, M., Monin, M. L., Gyapay, G., Lechner, D., Gonzalez, M., Depienne, C., Mochel, F., Lavie, J., Schols, L., Lacombe, D., Yahyaoui, M., Al Abdulkareem, I., Zuchner, S., Yamashita, A., Benomar A., Goizet, C., Durr A., Gleeson, J. G., Darios, F., Brice, A., and Stevanin, G. (2012) Alteration of fatty-acid-metabolizing enzymes affects mitochondrial form and function in hereditary spastic paraplegia. *Am. J. Hum. Genet.* **91,** 1051–1064
17. Blackstone, C. (2012) Cellular pathways of hereditary spastic paraplegia. *Annu. Rev. Neurosci.* **35,** 25–47
18. Shimoi, W., Ezawa, I., Nakamoto, K., Uesaki, S., Gabreski, G., Aridor, M., Yamamoto, A., Nagahama, M., Tagaya, M., and Tani, K. (2005) p125 is localized in endoplasmic reticulum exit sites and involved in their organization. *J. Biol. Chem.* **280,** 10141–10148
19. Ihara, M., Kinoshita, A., Yamada, S., Tanaka, H., Tanigaki, A., Kitano, A., Goto, M., Okubo, K., Nishiyama, H., Ogawa, O., Takahashi, C., Itohara, S., Nishimune, Y., Noda, M., and Kinoshita, M. (2005) Cortical organization by the septin cytoskeleton is essential for structural and mechanical integrity of mammalian spermatozoa. *Dev. Cell* **8,** 343–352
20. Iinuma, T., Shiga, A., Nakamoto, K., O'Brien, M. B., Aridor, M., Arimitsu, N., Tagaya, M., and Tani, K. (2007) Mammalian Sec16/p250 plays a role in membrane traffic from the endoplasmic reticulum. *J. Biol. Chem.* **282,** 17632–17639
21. Arimitsu, N., Kogure, T., Baba, T., Nakao, K., Hamamoto, H., Sekimizu, K., Yamamoto, A., Nakanishi, H., Taguchi, R., Tagaya, M., and Tani, K. (2011) p125/Sec23-interacting protein (Sec23ip) is required for spermiogenesis. *FEBS Lett.* **585,** 2171–2176
22. Baba, T., Yamamoto, A., Tagaya, M., and Tani, K. (2013) A lysophospholipid acyltransferase antagonist, CI-976, creates novel membrane tubules marked by intracellular phospholipase A$_1$ KIAA0725p. *Mol. Cell. Biochem.* **376,** 151–161
23. Inoue, H., Baba, T., Sato, S., Ohtsuki, R., Takemori, A., Watanabe, T., Tagaya, M., and Tani, K. (2012) Roles of SAM and DDHD domains in mammalian intracellular phospholipase A$_1$ KIAA0725p. *Biochim. Biophys. Acta* **1823,** 930–939
24. Suzuki, J., Sukezane, T., Akagi, T., Georgescu, M. M., Ohtani, M., Inoue, H., Jat, P. S., Goff, S. P., Hanafusa, H., and Shishido, T. (2004) Loss of c-abl facilitates anchorage-independent growth of p53- and RB-deficient primary mouse embryonic fibroblasts. *Oncogene* **23,** 8527–8534
25. Ishihara, N., Jofuku, A., Eura, Y., and Mihara, K. (2003) Regulation of mitochondrial morphology by membrane potential, and DRP1-dependent

division and FZO1-dependent fusion reaction in mammalian cells. *Biochem. Biophys. Res. Commun.* **301,** 891–898
26. Smirnova, E., Griparic, L., Shurland, D. L., and van der Bliek, A. M. (2001) Dynamin-related protein Drp1 is required for mitochondrial division in mammalian cells. *Mol. Biol. Cell* **12,** 2245–2256
27. Zhao, J., Liu, T., Jin, S., Wang, X., Qu, M., Uhlén, P., Tomilin, N., Shupliakov, O., Lendahl, U., and Nistér, M. (2011) Human MIEF1 recruits Drp1 to mitochondrial outer membranes and promotes mitochondrial fusion rather than fission. *EMBO J.* **30,** 2762–2778
28. Rizzo, M. A., Shome, K., Watkins, S. C., and Romero, G. (2000) The recruitment of Raf-1 to membranes is mediated by direct interaction with phosphatidic acid and is independent of association with Ras. *J. Biol. Chem.* **275,** 23911–23918
29. Bligh, E. G., and Dyer, W. J. (1959) A rapid method for total lipid extraction and purification. *Can. J. Biochem. Physiol.* **37,** 911–917
30. Fawcett, D. W. (1970) A comparative view of sperm ultrastructure. *Biol. Reprod.* **2,** Suppl. 2, 90–127
31. Russell, L. D. (1990) *Histological and Histopathological Evaluation of the Testis*, pp. 119–161, Cache River Press, Clearwater, FL
32. Imai, H., Hakkaku, N., Iwamoto, R., Suzuki, J., Suzuki, T., Tajima, Y., Konishi, K., Minami, S., Ichinose, S., Ishizaka, K., Shioda, S., Arata, S., Nishimura, M., Naito, S., and Nakagawa, Y. (2009) Depletion of selenoprotein GPx4 in spermatocytes causes male infertility in mice. *J. Biol. Chem.* **284,** 32522–32532
33. Schneider, M., Förster, H., Boersma, A., Seiler, A., Wehnes, H., Sinowatz, F., Neumüller, C., Deutsch, M. J., Walch, A., Hrabé de Angelis, M., Wurst, W., Ursini, F., Roveri, A., Maleszewski, M., Maiorino, M., and Conrad M. (2009) Mitochondrial glutathione peroxidase 4 disruption causes male infertility. *FASEB J.* **23,** 3233–3242
34. Huh, W. K., Falvo, J. V., Gerke, L. C., Carroll, A. S., Howson, R. W., Weissman, J. S., and O'Shea, E. K. (2003) Global analysis of protein localization in budding yeast. *Nature* **425,** 686–691
35. Connerth, M., Tatsuta, T., Haag, M., Klecker, T., Westermann, B., and Langer, T. (2012) Intramitochondrial transport of phosphatidic acid in yeast by a lipid transfer protein. *Science* **338,** 815–818
36. Cowell, C. F., Döppler, H., Yan, I. K., Hausser, A., Umezawa, Y., and Storz, P. (2009) Mitochondrial diacylglycerol initiates protein-kinase D1-mediated ROS signaling. *J. Cell Sci.* **122,** 919–928
37. Jin, J. K., Kim, N. H., Lee, Y. J., Kim, Y. S., Choi, E. K., Kozlowski, P. B., Park, M. H., Kim, H. S., and Min do, S. (2006) Phospholipase D1 is up-regulated in the mitochondrial fraction from the brains of Alzheimer's disease patients. *Neurosci. Lett.* **407,** 263–267
38. Watanabe, T., Chuma, S., Yamamoto, Y., Kuramochi-Miyagawa, S., Totoki, Y., Toyoda, A., Hoki, Y., Fujiyama, A., Shibata, T., Sado, T., Noce, T., Nakano, T., Nakatsuji, N., Lin, H., and Sasaki, H. (2011) MITOPLD is a mitochondrial protein essential for nuage formation and piRNA biogenesis in the mouse germline. *Dev. Cell* **20,** 364–375
39. Pillai, R. S., and Chuma, S. (2012) piRNAs and their involvement in male germline development in mice. *Dev. Growth Differ.* **54,** 78–92
40. Hales, K. G., and Fuller, M. T. (1997) Developmentally regulated mitochondrial fusion mediated by a conserved, novel, predicted GTPase. *Cell* **90,** 121–129
41. Honda, S., and Hirose, S. (2003) Stage-specific enhanced expression of mitochondrial fusion and fission factors during spermatogenesis in rat testis. *Biochem. Biophys. Res. Commun.* **311,** 424–432
42. Schuurs-Hoeijmakers, J. H., Geraghty, M. T., Kamsteeg, E. J., Ben-Salem, S., de Bot, S. T., Nijhof, B., van de Vondervoort, I. I., van der Graaf, M., Nobau, A. C., Otte-Höller, I., Vermeer, S., Smith, A. C., Humphreys, P., Schwartzentruber, J., FORGE Canada Consortium., Ali, B. R., Al-Yahyaee, S. A., Tariq, S., Pramathan, T., Bayoumi, R., Kremer, H. P., van de Warrenburg, B. P., van den Akker, W. M., Gilissen, C., Veltman, J. A., Janssen, I. M., Vulto-van Silfhout, A. T., van der Velde-Visser, S., Lefeber, D. J., Diekstra, A., Erasmus, C. E., Willemsen, M. A., Vissers, L. E., Lammens, M., van Bokhoven, H., Brunner, H. G., Wevers, R. A., Schenck, A., Al-Gazali, L., de Vries, B. B., and de Brouwer, A. P. (2012) Mutations in DDHD2, encoding an intracellular phospholipase A_1, cause a recessive form of complex hereditary spastic paraplegia. *Am. J. Hum. Genet.* **91,** 1073–1081
43. Gonzalez, M., Nampoothiri, S., Kornblum, C., Oteyza, A. C., Walter, J., Konidari, I., Hulme, W., Speziani, F., Schöls, L., Züchner, S., and Schüle, R. (2013) Mutations in phospholipase DDHD2 cause autosomal recessive hereditary spastic paraplegia (SPG54). *Eur. J. Hum. Genet.* **21,** 1214–1218
44. Douglas, D. S., Moran, J. L., Bermingham, J. R. Jr., Chen, X. J., Brindley, D. N., Soliven, B., Beier, D. R., and Popko, B. (2009) Concurrent Lpin1 and Nrcam mouse mutations result in severe peripheral neuropathy with transitory hindlimb paralysis. *J. Neurosci.* **29,** 12089–12100
45. Nadra, K., de Preux Charles, A. S., Médard, J. J., Hendriks, W. T., Han, G. S., Grès, S., Carman, G. M., Saulnier-Blache, J. S., Verheijen, M. H., and Chrast, R. (2008) Phosphatidic acid mediates demyelination in Lpin1 mutant mice. *Genes Dev.* **22,** 1647–1661
46. Mul, J. D., Nadra, K., Jagalur, N. B., Nijman, I. J., Toonen, P. W., Médard, J. J., Grès, S., de Bruin, A., Han, G. S., Brouwers, J. F., Carman, G. M., Saulnier-Blache, J. S., Meijer, D., Chrast, R., and Cuppen, E. (2011) A hypomorphic mutation in Lpin1 induces progressively improving neuropathy and lipodystrophy in the rat. *J. Biol. Chem.* **286,** 26781–26793